



LLIC: Large Receptive Field Transform Coding with Adaptive Weights for Learned Image Compression

Wei Jiang , Peirong Ning , Jiayu Yang , Yongqi Zhai , Feng Gao , *Member, IEEE*,
Ronggang Wang , *Member, IEEE*

Abstract—The effective receptive field (ERF) plays an important role in transform coding, which determines how much redundancy can be removed during transform and how many spatial priors can be utilized to synthesize textures during inverse transform. Existing methods rely on stacks of small kernels, whose ERFs remain insufficiently large, or heavy non-local attention mechanisms, which limit the potential of high-resolution image coding. To tackle this issue, we propose Large Receptive Field Transform Coding with Adaptive Weights for Learned Image Compression (LLIC). Specifically, for the *first time* in the learned image compression community, we introduce *a few* large kernel-based depth-wise convolutions to reduce more redundancy while maintaining modest complexity. Due to the wide range of image diversity, we further propose a mechanism to augment convolution adaptability through the self-conditioned generation of weights. The large kernels cooperate with non-linear embedding and gate mechanisms for better expressiveness and lighter point-wise interactions. Our investigation extends to refined training methods that unlock the full potential of these large kernels. Moreover, to promote more dynamic inter-channel interactions, we introduce an adaptive channel-wise bit allocation strategy that autonomously generates channel importance factors in a self-conditioned manner. To demonstrate the effectiveness of the proposed transform coding, we align the entropy model to compare with existing transform methods and obtain models LLIC-STF, LLIC-ELIC, and LLIC-TCM. Extensive experiments demonstrate that our proposed LLIC models have significant improvements over the corresponding baselines and reduce the BD-Rate by 9.49%, 9.47%, 10.94% on Kodak over VTM-17.0 Intra, respectively. Our LLIC models achieve state-of-the-art performances and better trade-offs between performance and complexity.

Index Terms—Transform coding, Learned image compression.

I. INTRODUCTION

Learned image compression [1]–[6] has become an active research area in recent years. Several models [7]–[15] have surpassed the advanced non-learned image codec Versatile Video Coding (VVC) Intra [16]. Most learned image compression models are based on variational autoencoders (VAEs) [17]. In this framework, an analysis transform first converts the input image to a latent representation, which is then quantized for entropy coding. A synthesis transform subsequently maps the quantized latent representation back to pixels. The advantages

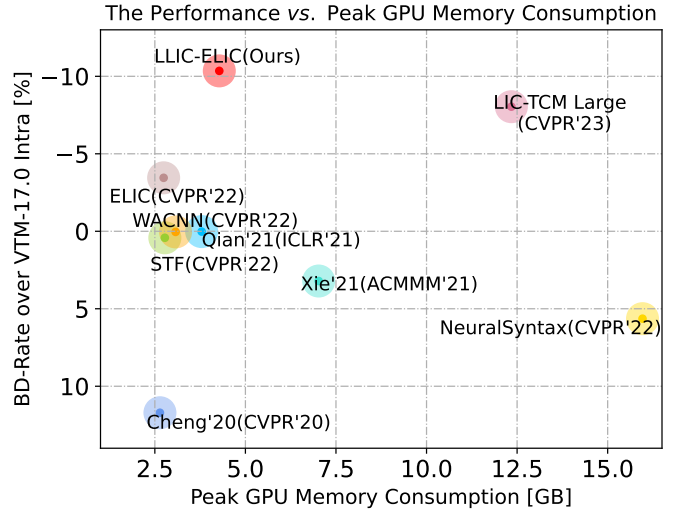


Fig. 1. BD-Rate-peak GPU Memory Consumption during testing on CLIC Pro Valid [19] with 2K resolution. Our LLIC-ELIC achieves a better trade-off between performance and GPU memory consumption.

of learned image compression over non-learned codecs are the end-to-end optimization and *non-linear* transform coding [18].

Recent improvements in the rate-distortion performance of learned image compression can be attributed to advancements in nonlinear transform coding [18]. The inherent non-linearity of such coding empowers the conversion of an input image to a more compact latent representation, typically requiring fewer bits for compression. The receptive field plays a crucial role in transform coding because it determines the maximum amount of redundancy that can be removed and the compactness of the latent representation. Furthermore, a large receptive field facilitates the generation of more accurate textures from more spatial priors during the synthesis transform. The effective receptive field is particularly important for high-resolution image coding due to the presence of more spatial correlations. For instance, in VVC, the largest size of coding unit is 128×128 (64×64 in High Efficiency Video Coding), ensuring that long-range dependencies can be captured in high-resolution images. Most earlier nonlinear transform coding techniques [1], [3]–[5], [9], [11]–[14], [20]–[23] rely on stacks of small kernels (e.g., 3×3 , 5×5) to enlarge the receptive field. However, the effective receptive fields (ERFs) [24] of stacks of small kernels remain limited, as illustrated in Fig. 8. To enlarge the receptive field, non-local attention [15], [25], [26] has been employed; however, its inherent quadratic complexity limits the potential for high-resolution image coding. Overall, enlarging

Wei Jiang, Peirong Ning, Jiayu Yang, Yongqi Zhai, Ronggang Wang are with Shenzhen Graduate School, Peking University, 518055 Shenzhen, China (email: wei.jiang1999@outlook.com).

Yongqi Zhai and Ronggang Wang are with Peng Cheng Laboratory, 518000 Shenzhen, China (email: rgwang@pkusz.edu.cn).

Feng Gao is with the School of Arts, Peking University, 100871, Beijing, China.

Ronggang Wang is the corresponding author.

the effective receptive field of nonlinear transform coding with acceptable complexity remains a challenge.

To our knowledge, large kernel design with the aim of achieving a large receptive field for transform coding has been overlooked. Could the application of a few larger kernels potentially confers advantages over the conventional approach of integrating numerous smaller kernels in transform coding? Additionally, due to the wide range of image diversity, the optimal transform coding for each image may differ. Compared with existing attention-based or transformer-based transform coding techniques [7], [8], [12], [15], [20], [26], the fixed convolutional weights used during testing are less flexible and adaptive. Based on above considerations, we introduce a novel Spatial Transform Block (STB) with large receptive fields and adaptability. Specifically, for the *first* time in the learned image compression community, we propose the application of depth-wise large kernels whose sizes range from 9×9 to 11×11 to achieve a good trade-off between performance and efficiency. To enhance the *adaptability* of convolution weights, we propose generating depth-wise kernel weights by using the input feature as the condition with a progressive down-sampling strategy. To argument the non-linearity of the transform, we propose the depth-wise residual block for non-linear embedding. Moreover, a gate block is proposed for low-complexity point-wise interactions. We also propose a simple yet effective training technique that uses large patches to fully exploit the potential of large kernels. Thanks to the proposed spatial transform with large receptive fields and adaptability, our proposed transform coding achieves much larger effective receptive fields with smaller depth, as illustrated in Fig. 8. A more widely distributed green area indicates a larger ERF. A larger ERF indicates that more spatial contextual information is captured and utilized during the transform, thus making the latent representation more compact, which means that it requires fewer bits to compress an image. Moreover, the complexity of the proposed transform coding method is still modest.

Large adaptive depth-wise kernels are effective at reducing spatial redundancy; however, the adaptive interactions among channels are limited. Given the heterogeneity of information carried by different channels in a latent representation, a more targeted approach that dynamically allocates more bits to more informative channels can enhance coding efficiency. To address this issue, inspired by Channel Attention [27], we propose a novel adaptive channel transform block (CTB). The CTB shares the macro architecture of the STB, where non-linear embedding and gate block are also employed. Specifically, it generates channel importance factors through a condition-based, progressive down-sampling process, subsequently applying these factors to the latent representation to modulate channel-wise importance dynamically.

To validate the effectiveness of the proposed transform coding, we combine the proposed transform coding techniques with the entropy models of STF [8], ELIC [12], and LIC-TCM [15] and obtain the learned image compression models LLIC-STF, LLIC-ELIC, and LLIC-TCM for fair comparisons with existing state-of-the-art transform coding methods. Extensive experiments demonstrate that our models significantly

improve upon the corresponding baselines, especially on high-resolution images. Our LLIC models achieve state-of-the-art performance regarding rate-distortion performance and model complexity (Fig. 1, 10, Table I).

Our contributions are as follows:

- We introduce the Spatial Transform Block, utilizing 11×11 and 9×9 large receptive field transforms to reduce spatial redundancy. To our knowledge, this is the *first* time that large kernels have been employed in the learned image compression community.
- We propose the generation of depthwise convolutional weights in a progressive down-sampling manner, using the input itself as a condition, making CNNs adaptive.
- We propose the Channel Transform Block, which employs importance factors for self-conditioned adaptive channel-wise bit allocation in a progressive down-sampling manner, using the input itself as a condition.
- We propose the use of the Depth-wise Residual Bottleneck to enhance the non-linearity and the Gate block for efficient point-wise interaction.
- Extensive experiments demonstrate that our proposed LLIC-STF, LLIC-ELIC, and LLIC-TCM have significant improvements over corresponding baselines and reduce BD-Rate by 9.49%, 9.47%, and 10.94% on Kodak over VTM-17.0 Intra, respectively. Our LLIC models achieve state-of-the-art performances and better trade-off between performance and complexity.

II. RELATED WORKS

A. Learned Image Compression

Toderici *et al.* [28], [29] propose the first learned image compression model based on recurrent neural networks, which encodes the residual between the reconstruction and ground-truth iteratively. Currently, most of the end-to-end learned image compression models [1]–[5], [12], [13], [20] are based on auto-encoders, where the input image is first transformed to the latent space for entropy coding, and the decoded latent is inversely transformed to the RGB color space. To enhance the rate-distortion performance, Ballé *et al.* [3] introduce a hyper-prior for more accurate entropy coding. Context modeling [4] is also utilized to explore the correlations between current symbols and decoded symbols. Minnen *et al.* [4] employ pixel-cnn [30] for serial context prediction. He *et al.* [31] propose checkerboard context partition for parallel context modeling. Minnen *et al.* [5] propose conducting serial context modeling along the channel dimension for faster decoding. In addition, global context modeling [13], [14], [32] is also introduced to explore the correlations among distant symbols. Multi-dimensional context modeling is recently developed. He *et al.* [12] combine the checkerboard partition and channel-wise context modeling. Jiang *et al.* [13], [14] propose the multi-reference entropy modeling to capture the local, global, and channel-wise correlations in an entropy model.

B. Learned Transform Coding

The advantage of end-to-end learned image compression over non-learned codecs is its non-linear transform coding [18].

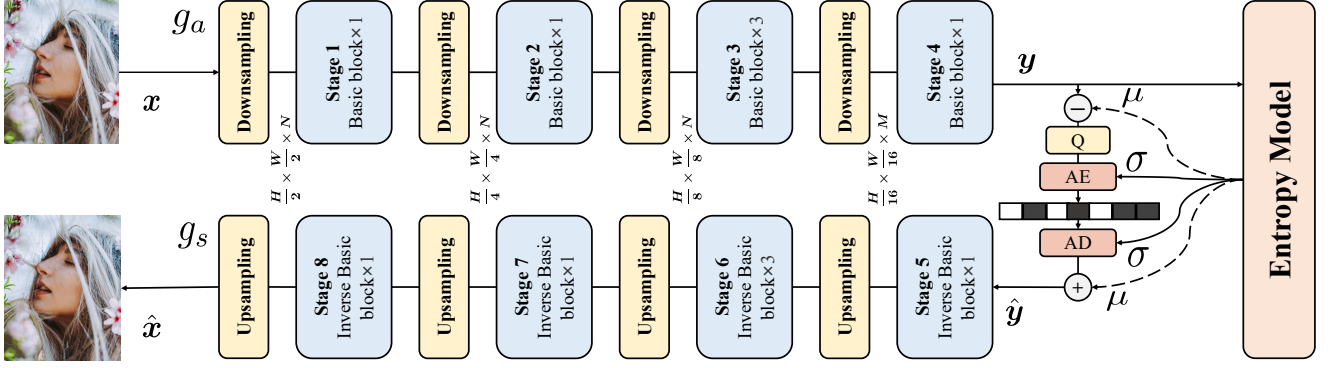


Fig. 2. Network architecture of our LLIC-STF, LLIC-ELIC, and LLIC-TCM. g_a is the analysis transform. g_s is the synthesis transform. Q is the quantization. μ and σ are the estimated mean and scale of latent \tilde{y} for probability estimation. Following baseline models, the latent representation y subtracts the means μ for quantization before arithmetic encoding (AE), and the decoded residual $Q(y - \mu)$ adds the means μ after arithmetic decoding (AD). $N = 192$, $M = 320$.

The transform plays an important role in improving the rate-distortion performance. For enhanced non-linearity, techniques such as generalized divisive normalization (GDN) [33] and Residual Bottleneck [34] have been utilized in learned image compression. Moreover, innovative normalization methods [35] have been proposed in recent years. Furthermore, Cheng *et al.* [20] suggest employing pixel shuffle for improved up-sampling. Various approaches [21], [36], [37] have been proposed for better interactions between high-frequency and low-frequency features. For example, Akbari *et al.* [36] propose employing octave convolution [38] to preserve more spatial structure of the information. Gao *et al.* [37] decompose the images into several layers with different frequency attributes for greater adaptability. Xie *et al.* [22] propose the adoption of invertible neural networks to reduce information loss during transform. Inspired by non-learned codecs, wavelet-like transform [39] is also introduced in recent years. In addition, non-local attention [26], simplified attention [20], and group-separated attention [32] are employed to reduce more spatial redundancy. However, such attention mechanisms are much heavier and lead to greater complexity. Transformers [40], [41] have been employed in several works [7], [8], [15], [42]–[45]. For example, Zou *et al.* [8], Lu *et al.* [44], Zhu *et al.* [7], and Wang *et al.* [45] stack swin-transformer [41] layers in transforms to reduce more redundancy. Liu *et al.* [15] employ mixed CNN-Transformer architectures for enhanced local and non-local interactions. The dynamic weights and large receptive field of transformers contribute significantly to the overall performance enhancement.

However, to our knowledge, the large kernels are still not explored in learned image compression. Employing large kernels may lead to larger effective receptive fields, which implies that more redundancy can be reduced. Furthermore, how to utilize large kernels without leading to high complexity is *non-trivial*.

III. METHOD

A. Problem Formulation

The formulation of end-to-end optimized image compression is first introduced. The fundamental architecture of this paradigm comprises three key components: an analysis transform g_a , a synthesis transform g_s , and an entropy model p .

The entropy model p computes the means μ and scales σ for probability estimation. The input image x is first transformed to the latent representation y via analysis transform g_a . The latent representation is quantized to \hat{y} for entropy coding. \hat{y} is inverse transformed to the reconstructed image \hat{x} via the synthesis transform g_s . To ensure the differentiability of the model during the training phase, the quantization operation is replaced by either the addition of uniform noise (AUN) [3] or the straight-through estimator (STE) [2]. Notably, adding uniform noise $u \sim \mathcal{U}(-0.5, 0.5)$ [3] to latent representation makes optimization of the compression model for rate-distortion performance equivalent to the minimization of the KL divergence (in VAEs [17]):

$$\begin{aligned} \mathcal{L} &= -(\mathcal{R} + \lambda \times \mathcal{D}) \\ &= \mathbb{E}_{q(\tilde{y}|x)} \left[\underbrace{\log p(x|\tilde{y})}_{\text{distortion}} + \underbrace{\log p(\tilde{y}) - \log q(\tilde{y}|x)}_{\text{rate}} \right]. \end{aligned} \quad (1)$$

$\log p(x|\tilde{y})$ is considered to be distortion because

$$p(x|\tilde{y}) = \mathcal{N}(x|\tilde{x}, (2\lambda)^{-1}\mathbf{1}), \quad (2)$$

which is the mean square error (MSE). $\mathbb{E}_{q(\tilde{y}|x)} \log p(\tilde{y})$ is the cross entropy, which is the theoretical bound of entropy coding.

$$q(\tilde{y}|x) = q(\tilde{y}|y) = \mathcal{U}(\tilde{y}|y - 0.5, y + 0.5) = 1. \quad (3)$$

Currently, most of the learned image compression models [3]–[5], [8], [12], [13], [20], [22] also incorporate hyper-priors [3]. The side information z is extracted from y using a hyper-prior network. The side information \tilde{z} or \hat{z} helps to estimate the entropy of latent \tilde{y} or \hat{y} . The loss function during training becomes

$$\begin{aligned} \mathcal{L} &= -(\mathcal{R} + \lambda \times \mathcal{D}) \\ &= \mathbb{E}_{q(\tilde{y}, \tilde{z}|x)} \left[\underbrace{\log p(x|\tilde{y})}_{\text{distortion}} + \underbrace{\log p(\tilde{y}|\tilde{z}) + \log p(\tilde{z})}_{\text{rate}} \right. \\ &\quad \left. - \underbrace{\log q(\tilde{y}|x) + \log q(\tilde{z}|y)}_0 \right]. \end{aligned} \quad (4)$$

Compared with traditional image codecs [16], [46]–[48], the advantage of the learned image compression is its *non-*

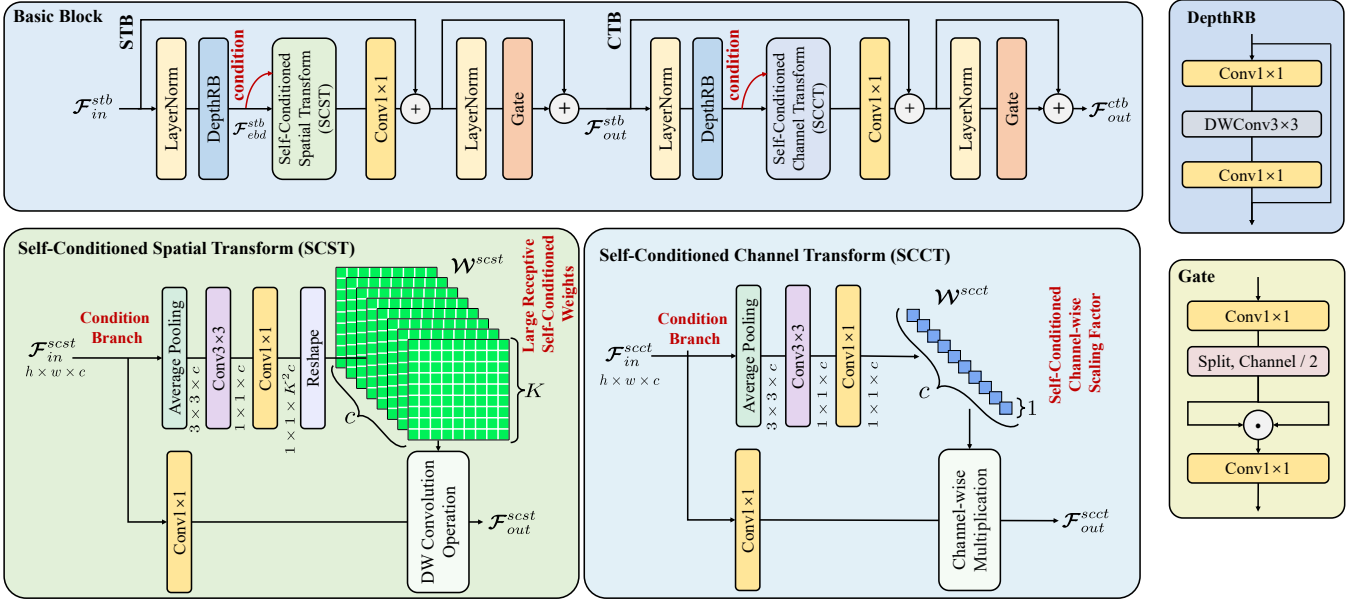


Fig. 3. Architecture of the proposed basic block. STB is the proposed Spatial Transform Block. CTB is the proposed Channel Transform Block. DepthRB is the depth-wise residual block for non-linear embedding. Gate is the proposed Gate Block. \mathcal{F}_{in}^{stb} is the input of STB. \mathcal{F}_{in}^{ctb} is the input of CTB. In STB, we employ *large* kernels to capture more spatial contexts, and the kernel size K is set to 11 or 9 in our method.

linear transform coding [18]. In such a framework, the analysis transform and synthesis transform play important roles.

First, the transform is employed to de-correlate the input image, effectively reducing correlations and thus enabling a more compact latent representation. This, in turn, contributes to a reduced bit-rate necessary for compression. Despite these advancements, the receptive fields of most current learned image compression models remain somewhat limited, leading to the persistence of certain redundancies within the latent representation. Moreover, the inflexibility of transform module weights during inference, due to their fixed nature, significantly impairs content adaptability, thereby constraining overall performance.

Second, from the perspective of generative models, the synthesis transform is conceptualized as a generator that plays a pivotal role in influencing the quality of the reconstructed image. A powerful and expressive synthesis transform has the capacity to produce finer details from the input latent representation $\hat{\mathbf{y}}$, enhancing the visual quality of the output.

Third, most of the analysis transforms down-sample the input four times, which makes the resolution of the latent representation \mathbf{y} much smaller than that of the input image \mathbf{x} . The complexity of image compression models is primarily attributable to transform coding. For instance, as demonstrated by Cheng'20 [20], the forward MACs (MACs) required by their model for an input image of size 768×512 reach 415.61 GMACs, in stark contrast to the mere 0.53 GMACs necessitated by the entropy model. Thus, the development of a more potent transform module that can minimize redundancies while maintaining a reasonable model complexity presents a considerable challenge.

These challenges, along with the potential to further enhance the rate-distortion performance of learned image compression, motivate us to design large receptive field transform coding with

self-conditioned adaptability for learned image compression.

B. Overview of Our Approach

The overall architecture of the proposed LLIC-STF, LLIC-ELIC, and LLIC-TCM is presented in Fig. 2 and Fig. 3. Our baseline models employ three types of state-of-the-art transform coding techniques. STF [8] employs transformers [41] for more compact latent representations. ELIC [12] employs residual convolutional layers and attention techniques [20] to enhance the non-linearity. LIC-TCM [15] employs mixed CNN-transformer architectures to focus on the local and non-local redundancies. For fair comparisons with existing transform coding techniques, the entropy models of LLIC-STF, LLIC-ELIC, and LLIC-TCM are aligned with the entropy models of STF [8], ELIC [12], and LIC-TCM [15], respectively.

Aligning with our baseline models and established methods [3]–[5], [13], [20], the proposed analysis and synthesis transforms in our work encompass four stages. Within each stage, the input undergoes either down-sampling or up-sampling through dedicated blocks. These down-sampling and up-sampling blocks incorporate a convolutional layer and a depth-wise residual bottleneck [12]. Subsequent to the sampling operations, the resultant features are propagated through basic blocks or their inverse counterparts. The basic block comprises two fundamental components: a Spatial Transform Block (STB) and a Channel Transform Block (CTB). In the inverse basic block, the architectural arrangement is reversed, with the positions of the STB and CTB interchanged. The structures of STB and CTB follow the classic architecture of Transformers [40], [41]. To ensure stable training, both the STB and CTB integrate layer normalization [49]. Internally, the STB and CTB employ a Depth-wise Residual Block (DepthRB) for non-linear embedding, coupled with the core transform blocks and a gated block to facilitate point-wise interactions.

C. Proposed Spatial Transform Block (STB)

The architecture of STB is shown in Figure 3. Depth Residual Block (DepthRB) is proposed for *non-linear* embedding. A Gate Block is proposed for efficient point-wise interactions with low complexity. We propose the Self-Conditioned Spatial Transform (SCST) to effectively reduce spatial redundancy. The overall process is formulated as:

$$\begin{aligned}\mathcal{F}_{ebd}^{stb} &= \text{DepthRB}(\text{Norm}(\mathcal{F}_{in}^{stb})), \\ \mathcal{F}_{scst}^{stb} &= \text{SCST}(\mathcal{F}_{ebd}^{stb}), \\ \mathcal{F}_{skip}^{stb} &= \text{Conv1} \times 1(\mathcal{F}_{scst}^{stb}) + \mathcal{F}_{in}^{stb}, \\ \mathcal{F}_{out}^{stb} &= \text{Gate}(\text{Norm}(\mathcal{F}_{skip}^{stb})) + \mathcal{F}_{skip}^{stb},\end{aligned}\quad (5)$$

where \mathcal{F}_{in}^{stb} is the input feature and \mathcal{F}_{out}^{stb} is the output feature.

1) *Nonlinear Embedding*: Previous works [8], [15], [40], [41] adopt one linear convolutional layer for embedding. In contrast to previous works, our STB uses a non-linear embedding method. We propose employing DepthRB. The architecture of DepthRB is presented in Figure 3, which contains a 1×1 convolutional layer, a 3×3 depth-wise convolutional layer, and a 1×1 convolutional layer. The use of depth-wise convolution helps to minimize complexity. The 3×3 depth-wise convolutional layer helps to aggregate more spatial information, and non-linearity enhances the expressiveness of the network.

2) *Self-Conditioned Spatial Transform (SCST)*: During the transform, the elimination of redundancies directly correlates with the compactness of the latent representation obtained. However, current state-of-the-art learned image compression models often fall short in terms of the size of their effective receptive fields, as depicted in Fig. 8. They [4], [5], [12], [20] usually employ 3×3 or 5×5 kernels. This limitation in receptive field size leaves unaddressed redundancies, thereby hampering the efficiency of compression. To achieve larger effective receptive fields, we propose employing large depth-wise kernels for analysis and synthesis transform. To our knowledge, this is the *first* attempt in the learned image compression community to apply large kernels for transform. In our proposed transform coding method, the kernel size is enlarged to $\{11, 11, 9, 9\}$ for different stages of analysis transform. The kernel sizes of the first two stages are larger because of the larger resolutions of the input features in the first two stages. The large-resolution features contain more spatial redundancies.

Although large kernels are employed in our proposed LLIC, the complexity is still modest due to the depth-wise connectivity. It is assumed that the large kernel size of a depth-wise convolution is K_L , the small kernel size of a vanilla convolution is K_S , and the input and output channels are N . The complexity of the large depth-wise convolution is $K_L^2 \times N$, and the complexity of the small vanilla convolution is $K_S^2 \times N^2$.

$$\begin{aligned}K_L^2 \times N &\geq K_S^2 \times N^2, \\ K_L &\geq K_S \sqrt{N}.\end{aligned}\quad (6)$$

N is 192 in our LLIC models and our baselines [3]–[5], [8], [12], [20], and $\sqrt{192} \approx 13.86$, indicating that a 11×11 depth-wise convolution is lighter than a 1×1 vanilla convolution.

In contrast to the existing methods that rely on transformer-based or attention-based transform coding techniques, the static convolutional layer weights present a limitation in harnessing the characteristics of the input image or features. To this end, we propose generating convolutional weights by treating the input itself as the condition in a progressive down-sampling manner. The condition branch in SCST is utilized to generate the self-conditioned adaptive weights. Specifically, the input feature $\mathcal{F}_{in}^{scst} \in \mathbb{R}^{c \times h \times w}$ is first average pooled to $\mathcal{F}_{pool}^{scst} \in \mathbb{R}^{c \times 3 \times 3}$, where c, h, w are the channel number, height, and width of \mathcal{F}_{in}^{scst} , respectively. The self-conditioned adaptive weights $\mathcal{W}^{scst} \in \mathbb{R}^{c \times K^2}$ are computed via the convolution between the average pooled feature $\mathcal{F}_{pool}^{scst}$ and the weights of the condition branch, where K is the kernel size.

The overall process of the proposed SCST is formulated as follows:

$$\begin{aligned}\mathcal{F}_{pool}^{scst} &= \text{AvgPool}(\mathcal{F}_{in}^{scst}), \\ \mathcal{W}^{scst} &= \text{Conv1} \times 1(\text{Conv3} \times 3(\mathcal{F}_{pool}^{scst})), \\ \mathcal{F}_{out}^{scst} &= \mathcal{W}^{scst} \otimes \text{Conv1} \times 1(\mathcal{F}_{in}^{scst}),\end{aligned}\quad (7)$$

where \mathcal{F}_{out}^{scst} is the output feature, \otimes is the convolution operation.

3) *Gate Mechanism*: In previous works [7], [8], the feed forward network (FFN) [40] is adopted for channel-wise interactions, which contains two linear layers and a GELU [50] activation function. The overall process of an FFN is

$$\begin{aligned}\mathcal{F}_{inc}^{gate} &= \text{Conv1} \times 1(\mathcal{F}_{in}^{gate}), \\ \mathcal{F}_{act}^{gate} &= \frac{1}{2} \mathcal{F}_{inc}^{gate} \left(1 + \tanh \left[\sqrt{\frac{2}{\pi}} \left(0.044715 (\mathcal{F}_{inc}^{gate})^3 \right) \right] \right), \\ \mathcal{F}_{out}^{gate} &= \text{Conv1} \times 1(\mathcal{F}_{act}^{gate}) + \mathcal{F}_{in}^{gate},\end{aligned}\quad (8)$$

where $\mathcal{F}_{in}^{gate} \in \mathbb{R}^{c \times h \times w}$ is the input feature and $\mathcal{F}_{out}^{gate} \in \mathbb{R}^{c \times h \times w}$ is the output feature. Following existing methods, the channel number of \mathcal{F}_{inc}^{gate} and \mathcal{F}_{act}^{gate} is $2c$. The first 1×1 convolutional layer increases the dimension of the input, and the second 1×1 convolutional layer decreases the dimension to the original dimension. GELU [50] is much more complex than ReLU [51] or LeakyReLU. The GELU function can be simplified as $\mathcal{F}_{inc}^{gate} \Phi(\mathcal{F}_{inc}^{gate})$ [52], which is quite similar to the gate mechanism. Replacing GELU with a gate mechanism leads to lower complexity, which inspired us to employ a gate block instead of an FFN. The architecture of our gate block is illustrated in Figure 3. Specifically, \mathcal{F}_{inc}^{gate} is split into two features $\mathcal{F}_1^{gate} \in \mathbb{R}^{c \times h \times w}$ and $\mathcal{F}_2^{gate} \in \mathbb{R}^{c \times h \times w}$ along the channel dimension. The activated feature \mathcal{F}_{act}^{gate} is obtained via the Hadamard product between \mathcal{F}_1^{gate} and \mathcal{F}_2^{gate} . The gate mechanism causes non-linearity, which is similar to GELU. The learnable 1×1 convolutional layer also makes the proposed gate mechanism more flexible. The overall process of the proposed gate block is

$$\begin{aligned}\mathcal{F}_{inc}^{gate} &= \text{Conv1} \times 1(\mathcal{F}_{in}^{gate}), \\ \mathcal{F}_1^{gate}, \mathcal{F}_2^{gate} &= \text{Split}(\mathcal{F}_{inc}^{gate}), \\ \mathcal{F}_{act}^{gate} &= \mathcal{F}_1^{gate} \odot \mathcal{F}_2^{gate}, \\ \mathcal{F}_{out}^{gate} &= \text{Conv1} \times 1(\mathcal{F}_{act}^{gate}) + \mathcal{F}_{in}^{gate}.\end{aligned}\quad (9)$$

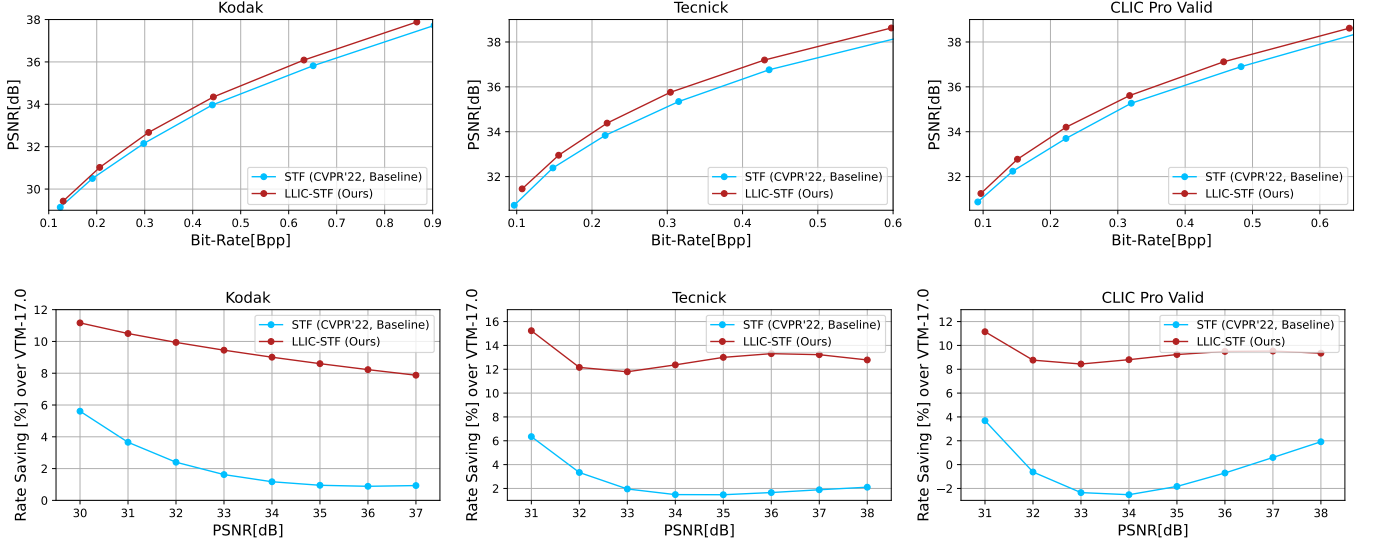


Fig. 4. PSNR-Bit-Rate curves and Rate saving-PSNR curves of our proposed LLIC-STF and its baseline STF [8]. The relative rate-saving curves are generated by first interpolating the discrete RD points with a cubic spline and then comparing the bitrates of different models at a fixed PSNR.

The complexity of an FFN is approximately $O(4c^2hw + 2chw)$, while the complexity of the proposed gate block is $O(3c^2hw + chw)$. The gate block is more efficient.

D. Proposed Channel Transform Block (CTB)

In the proposed Spatial Transform Block (STB), the kernel weights are connected in a depth-wise manner, necessitating the enhancement of interactions among channels. Compared to baseline models and existing learned image compression approaches, STB employs significantly larger kernels, enabling a more expansive receptive field at the same depth. This increased receptive field capacity provides an opportunity to further strengthen the interactions between channels. Our proposed CTB is illustrated in Figure 3. The architecture of CTB is similar to that of STB. The SCST in STB is replaced with Self-Conditioned Channel Transform (SCCT) to build the CTB. DepthRB for non-linear embedding and gate block are also employed. The overall process is formulated as

$$\begin{aligned}
 \mathcal{F}_{ebd}^{ctb} &= \text{DepthRB}(\text{Norm}(\mathcal{F}_{in}^{ctb})), \\
 \mathcal{F}_{scst}^{ctb} &= \text{SCCT}(\mathcal{F}_{ebd}^{ctb}), \\
 \mathcal{F}_{skip}^{ctb} &= \text{Conv1} \times 1 \left(\mathcal{F}_{scst}^{ctb} \right) + \mathcal{F}_{in}^{ctb}, \\
 \mathcal{F}_{out}^{ctb} &= \text{Gate}(\text{Norm}(\mathcal{F}_{skip}^{ctb})) + \mathcal{F}_{skip}^{ctb},
 \end{aligned} \tag{10}$$

where \mathcal{F}_{in}^{ctb} is the input feature and \mathcal{F}_{out}^{ctb} is the output feature.

1) *Self-Conditioned Channel Transform (SCCT)*: In STB, large receptive field kernels with self-conditioned adaptability are employed to reduce spatial redundancy. Due to the limited interactions among channels, Self-Conditioned Channel Transform (SCCT) is introduced to reduce channel-wise redundancy. It is important to recognize that different channels within a feature map carry varying levels of information. Some channels contain crucial information for reconstruction, while others may be less informative. By allocating more bits to critical channels

and fewer bits to non-critical channels, we can achieve more efficient utilization of the available bit-rate. To address this issue and inspired by Channel Attention [27], we propose generating adaptive channel factors to modify channel weights. The proposed SCCT contains a condition branch and a main branch. In the condition branch, the progressive down-sampling strategy is also adopted, which reduces information loss. The input feature \mathcal{F}_{in}^{scct} is employed as a condition. \mathcal{F}_{in}^{scct} is average pooled to reset the resolution and obtain $\mathcal{F}_{pool}^{scct} \in \mathbb{R}^{c \times 3 \times 3}$. The self-conditioned channel scaling factor $\mathcal{W}^{scct} \in \mathbb{R}^{c \times 1 \times 1}$ is computed via the convolution between $\mathcal{F}_{pool}^{scct}$ and the weights of the condition branch. The process is formulated as follows:

$$\begin{aligned}
 \mathcal{F}_{pool}^{scct} &= \text{AvgPool}(\mathcal{F}_{in}^{scct}), \\
 \mathcal{W}^{scct} &= \text{Conv1} \times 1 (\text{Conv3} \times 3 (\mathcal{F}_{pool}^{scct})), \\
 \mathcal{F}_{out}^{scct} &= \mathcal{W}^{scct} \odot \text{Conv1} \times 1 (\mathcal{F}_{in}^{scct}),
 \end{aligned} \tag{11}$$

where \mathcal{F}_{out}^{scct} is the output feature. Because the channel factor is dependent on the condition, our proposed channel transform is adaptive.

E. Improved Training Techniques

In previous works, the kernel sizes are 3×3 and 5×5 , which is not sufficient for redundancy reduction. In our STB, the kernel size is scaled up to 11×11 and 9×9 , which further enlarge the receptive field. However, it is *non-trivial* to fully exploit the potential of large kernels. Vanilla training strategies (using 256×256 patches) adopted by previous works [8], [12], [20] cannot fully utilize the large convolutional kernel. When using 256×256 patches, the resolutions of features during the analysis transform are $\{128 \times 128, 64 \times 64, 32 \times 32, \text{ and } 16 \times 16\}$, which are too small, especially 32×32 and 16×16 for the 11×11 and 9×9 kernels. To address this issue, we propose training using 512×512 patches. To mitigate the overhead, we adopt a two-stage training approach. First, we train the

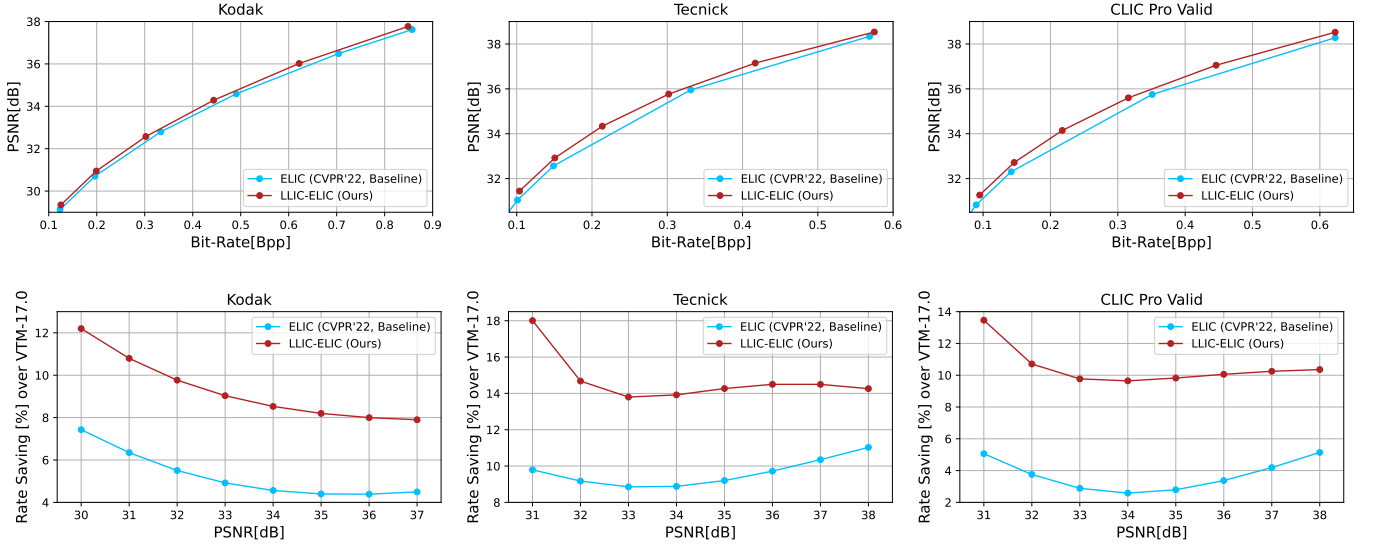


Fig. 5. PSNR-Bit-Rate curves and Rate saving-PSNR curves of our proposed LLIC-ELIC and its baseline ELIC [12].

models on 256×256 patches to establish a solid foundation. Subsequently, we train the models on 512×512 patches. This allows them to refine their understanding of larger-scale spatial relationships and fully exploit the potential of the large kernels. This approach is quite simple yet effective.

IV. EXPERIMENTS

A. Implementation Details

1) *Training dataset Preparation:* The proposed LLIC-STF, LLIC-ELIC, and LLIC-TCM are trained on 98939 images from COCO2017 [53], ImageNet [54], DIV2K [55], and Flickr2K [56]. The initial resolutions of these training images are greater than 512×512 . Following Ballé *et al* [3], in order to reduce compression artifacts that may be present in JPEG format images, JPEG images are further down-sampled with a randomized factor using the PIL library. This down-sampling process ensures that the minimum height or width of the images falls within the range of 512 to 584 pixels.

2) *Training Strategy:* Our proposed LLIC-STF, LLIC-ELIC, and LLIC-TCM are built on PyTorch 2.1 [57] and CompressAI 1.2.0b3 [58]. Equation 4 is employed as the loss function. Following existing methods [3]–[5], [12], [13], [20], the MSE and Multi-Scale Structural Similarity (MS-SSIM) are employed as distortion metrics during training for rate-distortion optimization. Following CompressAI [58], λ in Equation 4 is set to $\{18, 35, 67, 130, 250, 483\} \times 10^{-4}$ for MSE and $\{2.4, 4.58, 8.73, 16.64, 31.73, 60.5\}$ for MS-SSIM. The training process is conducted on 2 Intel(R) Xeon(R) Platinum 8260 CPUs and 8 Tesla V100-32G GPUs under the PyTorch distributed data parallel setting. During training, the batch size is set to 16. Each model is trained for 2 M steps. The initial learning rate is 10^{-4} . The learning rate decreases to 3×10^{-5} at 1.7 M steps, decreases to 10^{-5} at 1.8 M steps, decreases to 3×10^{-6} at 1.9 M steps, and finally decreases to 1.95 M steps. The training images are randomly cropped to 256×256

patches during the first 1.2M steps and randomly cropped to 512×512 patches during the remaining steps. Large patches are employed to improve the performance of large receptive field transform coding.

B. Test settings

1) *Performance Test Settings:* For models optimized for MSE, Peak Signal-to-Noise Ratio (PSNR) serves as the primary metric for quantifying distortion. The bits per pixel (Bpp) are utilized to measure bit-rate. The rate-distortion performances are measure on 5 widely used datasets, including

- Kodak [59], which contains 24 uncompressed images, is widely used in learned image compression community [1], [3]–[5], [7], [8], [12], [13], [20], [22], [36], [39], [60]–[63]. The resolution of the images in Kodak is 768×512 .
- Tecnick [64], which contains 100 uncompressed images, is utilized for performance evaluation in many previous works [4], [5], [15], [22], [65]. The resolution of images in Tecnick is 1200×1200 .
- CLIC Pro Valid [19] and CLIC 2021 Test [66] are the validation dataset of the 3rd Challenge on Learned Image Compression and the test dataset of the 4th Challenge on Learned Image Compression, respectively. CLIC Pro Valid contains 41 high-resolution images, and CLIC 2021 Test contains 60 high-resolution images. Due to the impact of Challenge on Learned Image Compression, CLIC datasets are widely employed for rate-distortion evaluation [8], [9], [11], [12], [15], [20]. The average resolution of images in CLIC datasets is approximately 2048×1370 .
- JPEG AI Test [67] is the test dataset of the MMSP 2020 Learning-based Image Coding Challenge and contains 16 images. The largest resolution of the images in JPEGAI Test is 3680×2456 .

These test datasets with different resolutions (from 768×512 to 3680×2456) offer a comprehensive evaluation of learned image compression models.

The Bjøntegaard delta rate (BD-Rate) [68] is utilized to rank the performance of the learned image compression models.

2) *Complexity Test Settings:* To comprehensively evaluate the complexities of various learned image compression models, 16 images with resolutions greater than 3584×3584 from the LIU4K test split [69] are selected as the complexity test images. These 16 images are further center cropped to $\{512 \times 512, 768 \times 768, 1024 \times 1024, 1536 \times 1536, 2048 \times 2048, 2560 \times 2560, 3072 \times 3072, 3584 \times 3584\}$ patches to cover the various resolutions of images that can be encountered in reality. The model complexities are evaluated from four perspectives, including the peak GPU memory during encoding and decoding, model Forward inference MACs, encoding time, and decoding time. The encoding and decoding times include the entropy coding and decoding times to better match practical applications and realistic scenarios.

C. Rate-Distortion Performance

1) *Quantitative Results:* We compare our proposed LLIC-STF, LLIC-ELIC, and LLIC-TCM with their baseline models STF [8], ELIC [12], and LIC-TCM [15], recent learned image compression models [5], [7], [9]–[11], [20], [22], [23], [63], [65], [70], and the non-learned image codec VTM-17.0 Intra [16]. The rate-distortion curves and rate-savings-distortion curves are illustrated in Fig. 4, Fig. 5, and Fig. 6. The BD-Rate reductions are presented in Table I. VTM-17.0 under the *encoder_intra_vtm.cfg* in the YUV444 color space is employed as an anchor.

Compared with the baseline model STF [8], our LLIC-STF achieves superior performance across all bit-rate tiers. Specifically, LLIC-STF achieves average enhancements of 0.33, 0.47, 0.40, 0.50, and 0.62 dB in PSNR over STF across Kodak [59], Tecnick [64], CLIC Pro Valid [19], CLIC 2021 Test, and JPEGAI Test [67], respectively. Our LLIC-STF decreases the bitrate by 7.2%, 10.88%, 9.81%, 11.01%, 12.34% on these datasets when the anchor is STF.

Compared with baseline model ELIC [12], LLIC-ELIC shows markedly enhanced efficacy across all evaluated bit-rates. Our proposed LLIC-ELIC yields average improvements of 0.19, 0.25, 0.29, 0.21, 0.39 dB PSNR compared to ELIC on Kodak [59], Tecnick [64], CLIC Pro Valid [19], CLIC 2021 Test, and JPEGAI Test [67], respectively. Our LLIC-ELIC decreases the bitrate by 4.25%, 5.66%, 7.11%, 4.80%, and 8.54% on these datasets when the anchor is ELIC.

When comparing LLIC-TCM with LIC-TCM models, it is pertinent to highlight the significant performance uplift over the LIC-TCM Middle, noting that the MACs of our LLIC-TCM is 321.93 G and the MACs of the LIC-TCM Middle is 415.2 G. The MACs of LIC-TCM Large is 717.08 G. Our LLIC-TCM performs much better than LIC-TCM Middle and slightly better than LLIC-TCM Large on Kodak. Our proposed LLIC-TCM decreases the bitrate by 3% more than LIC-TCM Middle and 1% more than LIC-TCM Large. Our LLIC-TCM performs much better than LIC-TCM models on *high-resolution* images. Our LLIC-TCM decreases the bitrate by 6%, 4% more than LIC-TCM Middle and 3.5%, and 2.4% more than LIC-TCM Large on Tecnick and CLIC Pro Val, respectively. Our LLIC-

TCM outperforms LIC-TCM Large with only half the MACs of LIC-TCM Large.

2) *Qualitative Results:* Fig. 7 illustrates the example of reconstructed Kodim07 of our proposed models, WACNN, STF [8], Xie'21 [22], and VTM-17.0 Intra. The PSNR value of the image reconstructed by our proposed models is 1 dB higher than that of the image reconstructed by VTM-17.0 Intra. Compared with STF, VTM-17.0 Intra and other codecs, our proposed models can retain more details. Images reconstructed by our proposed LLIC have higher subjective quality.

D. Computational Complexity

GPU Memory Consumption-Image Resolution, Forward MACs-Image Resolution, Encoding Time-Image Resolution, and Decoding Time-Image Resolution curves are presented in Fig. 10. We compare our proposed LLIC-STF, LLIC-ELIC, and LLIC-TCM with their baseline models STF [8], ELIC [12], and LIC-TCM Large [15] and recent learned image compression models [20], [22], [23], [63], [70]. Overall, our proposed transform coding method enhances the model performance while exhibiting modest GPU memory, forward inference MACs, and fast encoding and decoding speeds.

1) *Testing GPU Memory Consumption Comparison:* Compared with existing recent learned image compression models Xie'21 [22], Entroformer [70], and NeuralSyntax [71], our proposed LLIC transform coding consumes much less GPU memory. When compressing 3072×3072 images, the peak GPU memory of our proposed LLIC models is approximately 10 GB, while the GPU memory consumption of Xie'21 [22] is over 20 GB. Compared to the baseline models STF [8] and ELIC [12], our proposed LLIC-STF and LLIC-ELIC do not add much GPU memory overhead when compressing low-resolution images. The GPU memory consumptions of STF, ELIC, LLIC-STF, and LLIC-ELIC are very similar for low-resolution images. It should be emphasized that our LLIC-STF and LLIC-ELIC have great performance improvements over STF [8] and ELIC [12], which illustrates the superiority of our approach. Compared to the baseline model LIC-TCM Large [15], our LLIC-TCM significantly reduces the GPU memory consumption with better rate-distortion performance. When compressing and decompressing 2048×2048 images, the GPU memory consumption of our proposed LLIC-TCM is only $\frac{1}{3}$ of the GPU memory consumption of LIC-TCM Large. When compressing 3072×3072 images, the GPU memory consumption of our proposed LLIC-TCM is only $\frac{1}{4}$ of the GPU memory consumption of LIC-TCM Large. The curve of the GPU memory consumed by our LLIC-TCM as the resolution grows is much flatter. The GPU memory overhead is a very important measure of model complexity because, once the amount of GPU memory required for encoding or decoding exceeds the GPU memory capacity of the machine, it is no longer possible to encode and decode images. The lower GPU memory consumption indicates that our proposed LLIC-STF, LLIC-ELIC, and LLIC-TCM have lower complexity and are highly suitable for high-resolution image compression.

2) *Forward Inference MACs Comparison:* The forward inference MACs of the learned image compression models are

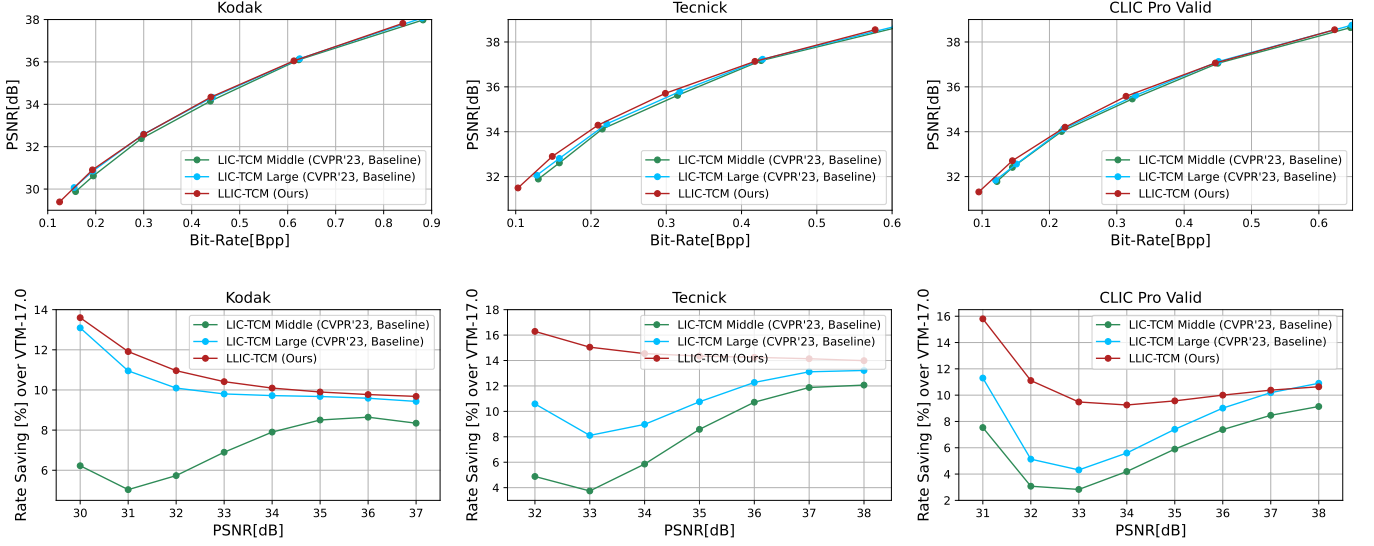


Fig. 6. PSNR-Bit-Rate curves and Rate saving-PSNR curves of our proposed LLIC-TCM and its baseline LIC-TCM [15]. We highlight the performance improvements over LIC-TCM Middle because the MACs of our LLIC-TCM is 321.93 G and the MACs of LIC-TCM Middle is 415.2 G on Kodak. The MACs of LIC-TCM Large is 717.08 G on Kodak. Our LLIC-TCM also outperforms LIC-TCM Large with only half the MACs of LIC-TCM Large.

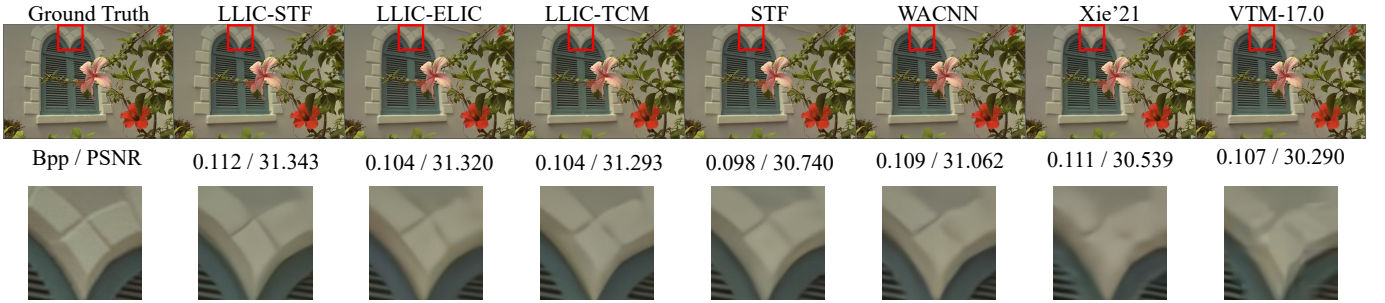


Fig. 7. Visualization of the reconstructed Kodim07 from the Kodak dataset. The metrics are [bpp↓/PSNR↑]. We compare our LLIC-STF, LLIC-ELIC, and LLIC-TCM with STF [8], WACNN [8], Xie'21 [22], and VTM-17.0 Intra [16].

computed through the fvcure, DeepSpeed, and Ptflops libraries. Because the flops evaluation libraries are not very accurate, when evaluating one model, we compute the output values of fvcure, Deepspeed, and Ptflops, and we take the average of the two closest values as the final result. Compared with the recent learned image compression models Cheng'20 [20], Xie'21 [22], Entroformer [70], and NeuralSyntax [23], our proposed LLIC-STF, LLIC-ELIC and LLIC-TCM demonstrate remarkable reductions in forward inference MACs. Notably, the forward MACs required for our LLIC models to compress images of dimensions 2048×2048 are approximately one-fourth of those reported for NeuralSyntax. Compared with the baseline models STF [8] and ELIC [12], our LLIC-STF and LLIC-ELIC have slightly higher forward MACs. Considering the performance gains of our proposed LLIC-STF and LLIC-ELIC over STF [8], and ELIC [12], it is worthwhile to increase the forward MACs a bit. In addition, the forward MACs of our proposed LLIC models are approximately 74% of the forward MACs of Cheng'20 [20] when compressing 2048×2048 images. Compared to the baseline model LIC-TCM Large, our proposed LLIC-TCM significantly reduces the forward MACs.

The forward MACs of our proposed LLIC-TCM is only 45% of the forward MACs of LIC-TCM Large when compressing 2048×2048 images and compressing 3072×3072 images. Compared with the mixed CNN-Transformer-based transform coding of LIC-TCM Large, our proposed large receptive field transform coding is more powerful and light-weight.

3) Encoding and Decoding Time Comparison: Because our LLIC-STF, LLIC-ELIC, and LLIC-TCM employ parallel entropy models, they encode and decode much faster than Cheng'20 [20], Xie'21 [22], Qian'21 [63], Entroformer [70] and NeuralSyntax [23]. Specifically, when compressing a 768×768 image, the encoding times of Cheng'20 and Xie'21 exceed 3s, the encoding times of Qian'21 and Entroformer exceed 40s, the decoding times of Cheng'20 and Xie'21 exceed 7s, and the decoding times of Qian'21 and Entroformer exceed 50s; meanwhile, the encoding and decoding times of our proposed LLIC models are approximately 0.06 ~ 0.1s and 0.1 ~ 0.12s, respectively. Compared to the baseline model STF [8], our proposed LLIC-STF is approximately as fast as STF [8]. Compared to the baseline model ELIC [12], our proposed LLIC-ELIC is approximately as fast as ELIC [12] on

TABLE I
BD-RATE (%) COMPARISON FOR PSNR (DB) AND MS-SSIM. THE ANCHOR IS VTM-17.0 INTRA.

| Methods | Venue | BD-Rate (%) w.r.t. VTM-17.0 Intra | | | | | |
|----------------------------|----------|-----------------------------------|---------------|---------------|---------------------|---------------------|------------------|
| | | Kodak [59] | | Tecnick [64] | CLIC Pro Valid [19] | CLIC 2021 Test [66] | JPEGAI Test [67] |
| | | PSNR | MS-SSIM | PSNR | PSNR | PSNR | PSNR |
| Cheng'20 [20] | CVPR'20 | +5.58 | -44.21 | +7.57 | +11.71 | +9.40 | +11.95 |
| Minnen'20 [5] | ICIP'20 | +3.23 | — | -0.88 | — | — | — |
| Qian'21 [63] | ICLR'21 | +10.05 | -39.53 | +7.52 | +0.02 | — | — |
| Xie'21 [22] | ACMMM'21 | +1.55 | -43.39 | -0.80 | +3.21 | +0.99 | +2.35 |
| Entroformer [70] | ICLR'22 | +4.73 | -42.64 | +2.31 | -1.04 | — | — |
| SwinT-Charm [7] | ICLR'22 | -1.73 | — | — | — | — | — |
| NeuralSyntax [23] | CVPR'22 | +8.97 | -39.56 | — | +5.64 | — | — |
| McQuic [9] | CVPR'22 | -1.57 | -47.94 | — | +6.82 | — | — |
| Contextformer [10] | ECCV'22 | -5.77 | -46.12 | -9.05 | — | — | — |
| Pan'22 [65] | ECCV'22 | +7.56 | -36.2 | +3.97 | — | — | — |
| NVTC [11] | CVPR'23 | -1.04 | — | — | — | -3.61 | — |
| STF as Baseline | | | | | | | |
| STF [8] | CVPR'22 | -2.48 | -47.72 | -2.75 | +0.42 | -0.16 | +1.54 |
| LLIC-STF | Ours | -9.49 | -49.11 | -13.06 | -9.32 | -11.44 | -11.15 |
| ELIC as Baseline | | | | | | | |
| ELIC [12] | CVPR'22 | -5.95 | -44.60 | -9.14 | -3.45 | -7.52 | -3.21 |
| LLIC-ELIC | Ours | -9.47 | -49.25 | -14.68 | -10.35 | -12.32 | -11.24 |
| LIC-TCM as Baseline | | | | | | | |
| LIC-TCM Middle [15] | CVPR'23 | -7.43 | — | -8.99 | -6.35 | — | — |
| LIC-TCM Large [15] | CVPR'23 | -10.14 | -48.94 | -11.47 | -8.04 | — | — |
| LLIC-TCM | Ours | -10.94 | -49.73 | -14.99 | -10.41 | -13.14 | -12.30 |

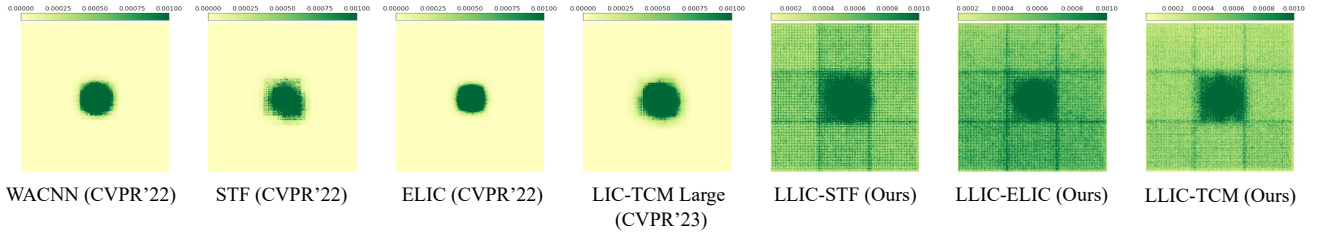


Fig. 8. Effective Receptive Fields (ERF) of analysis transforms g_a of WACNN, STF, ELIC, LIC-TCM Large and our proposed models on 24 Kodak images center-cropped to 512×512 . The ERF is visualized as the absolute gradients of the center pixel in the latent ($d\mathbf{y}/d\mathbf{x}$) with respect to the input image. Darker green colors represent larger gradients. A more widely distributed green area indicates a larger ERF. A larger ERF indicates that more spatial contextual information is captured and utilized during the transform.

low-resolution images. Our proposed LLIC-ELIC requires 20% more time and requires 7% to encode a 2048×2048 image. The added time to encode and decode the high-resolution images is worthwhile considering the performance improvement brought about by our proposed transform coding. Compared with LIC-TCM Large, our LLIC-TCM encodes and decodes much faster than the baseline model LIC-TCM Large. Overall, our proposed transform coding enhances model performance while achieving fast encoding and decoding speed.

E. Ablation Studies

1) *Settings*: Ablation studies are conducted on LLIC-STF. When conducting ablation experiments, we train each model

for 1.7M steps from scratch. The batch size is set to 16. We adopt the training strategy in section IV-A2. The results of ablation studies are in Table II. In Table II, “w/o Gate” means that the gate block is replaced by an FFN [40].

2) *Influence of Self-Conditioned Spatial Transform*: Although it is possible to increase the theoretical receptive field by continuously stacking network layers, it is likely that a small effective receptive field [24] will be obtained. Following Zhu *et al* [7], Effective Receptive Field (ERF) [24], [72] is employed to evaluate the influence of the proposed self-conditioned spatial transform, which utilizes large depth-wise convolutions. The ERF is visualized as the absolute gradient of the center pixel in the latent ($d\mathbf{y}/d\mathbf{x}$) with respect to

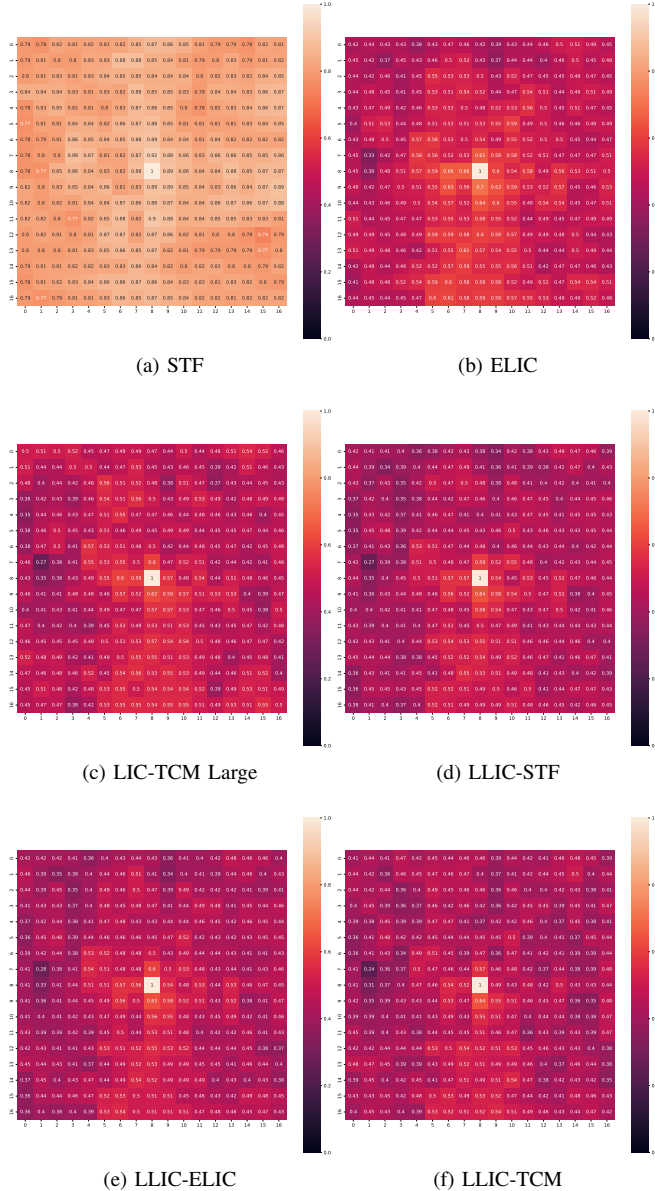


Fig. 9. Absolute value of the cosine similarity among latents. Note that the forward MACs of our LLIC models are only half of the forward MACs of LIC-TCM Large. Please zoom in for a better view.

the input image. The ERFs of our baseline models STF [8], ELIC [12], and LIC-TCM Large [15], our proposed LLIC-STF, LLIC-ELIC and LLIC-TCM are visualized in Fig. 8. Baseline model STF employs swin-transformer-based transform coding, ELIC employs CNN-Attention-based transform coding, and the recent LIC-TCM employs mixed CNN-Transformer-based transform coding. Compared with these different types of transform coding methods, it is obvious that our proposed LLIC-STF, LLIC-ELIC, and LLIC-TCM achieve much larger ERFs than their baselines. Larger ERFs indicate that our proposed large receptive field transform coding is able to remove more redundancy during the analysis transform, which makes our proposed models perform better than our baseline models.

To further demonstrate the advantages of large receptive fields, we compute the cosine similarity between the center

TABLE II
ABLATION STUDIES ON KODAK DATASET.

| Settings | BD-Rate (%) | Forward MACs (G) |
|-----------------------------|-------------|------------------|
| LLIC-STF Basic Block | | |
| STB + STB | -6.05 | 331.55 |
| CTB + CTB | -6.19 | 318.61 |
| only CTB | -5.05 | 214.90 |
| only STB | -4.19 | 221.29 |
| LLIC-STF w/o CTB | | |
| static weight | -2.58 | 221.26 |
| w/o DepthRB | -1.01 | 188.09 |
| w/o DepthRB & Gate | -0.18 | 198.83 |
| LLIC-STF w/o CTB | | |
| $K = \{5, 5, 5, 5\}$ | +0.05 | 216.28 |
| $K = \{7, 7, 7, 7\}$ | -2.46 | 217.62 |
| $K = \{9, 9, 9, 9\}$ | -3.38 | 219.29 |
| $K = \{11, 11, 9, 9\}$ | -4.19 | 221.29 |
| $K = \{11, 11, 11, 11\}$ | -4.42 | 221.62 |
| LLIC-STF | | |
| 256 × 256 patch | -4.64 | 325.00 |
| 512 × 512 patch | -7.85 | 325.00 |
| VTM-17.0 Intra | 0.00 | – |

latent and other latents in \mathbf{y} . The cosine similarity computation is performed on a 17×17 window obtained by center-cropping the latent representation. We compute cosine similarity on the Kodak dataset. The cosine similarities are averaged on 24 images from the Kodak dataset. The absolute cosine similarity map is visualized in Figure 9. According to Figure 9, our proposed method can reduce a large range of redundancies. For example, compared to the baseline methods STF, ELIC, and LIC-TCM, the similarity values of the 16-th rows of the similarity maps of the proposed method are lower. The lower similarity among distant latents can be attributed to larger effective receptive fields. A lower similarity indicates that a larger receptive field can reduce more spatial redundancy.

To further investigate the contribution of the proposed spatial transform block, the spatial transform block is removed or replaced in our ablation studies. Specifically, removing the STB leads to significant performance degradation. If the STB is replaced by CTB, the rate-distortion performance is still not as good as the performance of the model utilizing STBs and CTBs. This performance degradation indicates the necessity of employing the proposed spatial transform blocks for a more compact latent representation to enhance the rate-distortion performance.

In our models and baseline models, the analysis transform g_a and synthesis transform g_s involves four stages. The kernel size of each stage is denoted as $K = \{k_1, k_2, k_3, k_4\}$. To evaluate the contribution of large kernel, we set the kernel size $K = \{5, 5, 5, 5\}$, $K = \{7, 7, 7, 7\}$, $K = \{9, 9, 9, 9\}$, $K = \{11, 11, 9, 9\}$, and $K = \{11, 11, 11, 11\}$. The rate-distortion performances when utilizing various kernel sizes are shown in Table II. Clearly, increasing the size of the convolutional kernel keeps improving the rate-distortion perfor-

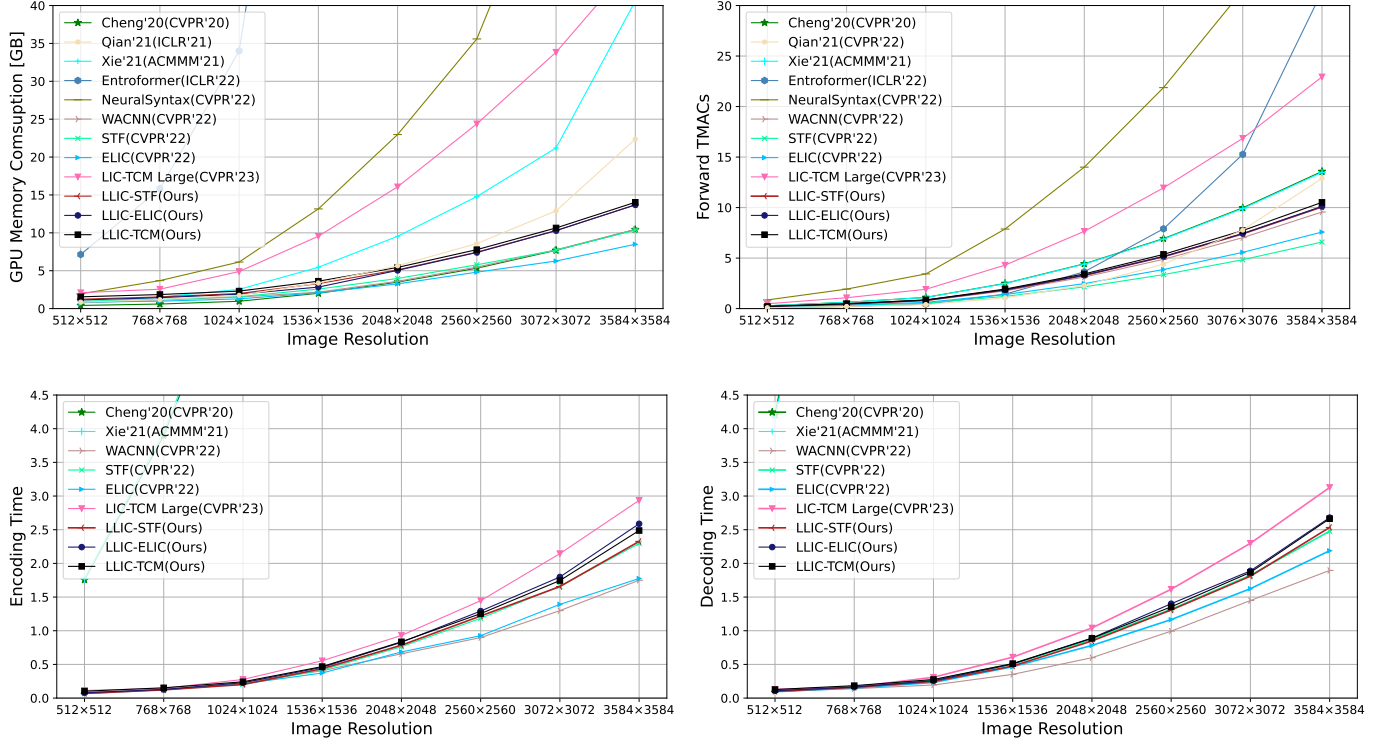


Fig. 10. GPU Memory Consumption-Image Resolution, Forward MACs-Image Resolution, Encoding Time-Image Resolution, Decoding Time-Image Resolution curves.

TABLE III
INFLUENCE OF KERNEL SIZE ON VARIOUS RESOLUTIONS.

| Kernel Size | BD-Rate (%) w.r.t. VTM-17.0 Intra | | | |
|------------------------|-----------------------------------|-------------------------------------|--|---|
| | Kodak (768×512) [59] | Tecnick (1200×1200) [64] | CLIC Pro Valid (2048×1370) [19] | JPEGAI Test (3680×2456) [67] |
| $K = \{5, 5, 5, 5\}$ | +0.05 | -1.17 | +1.72 | +1.13 |
| $K = \{7, 7, 7, 7\}$ | -2.46 | -4.27 | -1.63 | -2.91 |
| $K = \{9, 9, 9, 9\}$ | -3.38 | -6.89 | -3.47 | -5.12 |
| $K = \{11, 11, 9, 9\}$ | -4.19 | -8.17 | -4.33 | -7.76 |

mance of the model, However, the gains decrease. Increasing the kernel size K from $\{5, 5, 5, 5\}$ to $\{7, 7, 7, 7\}$ leads to the largest performance enhancement. The differences in the performance when utilizing $\{11, 11, 9, 9\}$ kernels and when utilizing $\{11, 11, 11, 11\}$ kernels are quite negligible. Therefore, in our proposed LLIC models, $K = \{11, 11, 9, 9\}$ is employed.

To analyze the relationship between the kernel size and compression performance with different resolutions, we conduct ablation studies on Kodak, Tecnick [64], CLIC Pro Valid [19], and JPEGAI Test [67]. The results are presented in Table III. As the resolution of the input image increases, the gap between the BD-Rate values of different kernels gradually increases. For example, when compressing 512×768 images (Kodak), the difference between $K = \{7, 7, 7, 7\}$ and $K = \{5, 5, 5, 5\}$ is -2.51% ; when compressing 1200×1200 (Tecnick) images, 2048×1370 (CLIC Pro Valid) images, and 3680×2456 (JPEGAI Test) images, the differences are -3.10% , -3.35% , -4.04% , respectively. The increased BD-Rate gap indicates that large kernel sizes is beneficial for high-

resolution image coding. Compared with low-resolution images, high-resolution images contain more *spatial redundancy*. For high-resolution images, pixels in a larger area are correlated with each other. In this case, the receptive field of the image compression model is crucial. If the receptive field is small, redundancy beyond its receptive field will be difficult to remove, especially when compressing high-resolution images. Therefore, we employ large depth-wise kernels to overcome the drawbacks of the previous methods while maintaining modest complexity. The large kernel leads to better performance when compressing high-resolution images.

Context adaptability also plays an important role in boosting the rate-distortion performance of learned image compression models. When the kernel weights are independent of the input feature, the rate-distortion becomes worse. The rate-distortion performance loss is approximately 1.6% . The performance degradations demonstrate the effectiveness of the proposed self-conditioned weight generation.

3) *Influence of Self-Conditioned Channel Transform*: The channel transform block is proposed for self-conditioned adaptive channel adjustment. In ablation studies, channel transform blocks are removed or replaced. Specifically, removing CTBs leads to significant performance degradation, and the rate-distortion performance of replacing CTBs with STBs is still not as good as the performance of the model utilizing CTBs and STBs. The performance degradation in ablation studies demonstrates the effectiveness and necessity of employing channel transform blocks in transform coding.

4) *Influence of DepthRB and Gate Mechanism*: We use LLIC-STF without CTBs to evaluate the effectiveness of the proposed DepthRB for nonlinear embedding. Compared with linear embedding, which employs a linear layer, our proposed DepthRB for non-linear embedding further enhances the rate-distortion performance. Non-linear embedding is more flexible than linear embedding. We also evaluate the effectiveness of the proposed gate block. Replacing the gate blocks with vanilla FFNs increases the complexity of the model but leads to performance degradation, which demonstrates the superiority of the proposed gate block.

5) *Influence of Large Patches for Training*: The 256×256 patches are insufficient for training. To fully exploit large kernels, the large training strategy is employed. Large patch training results in a performance increment of approximately 3%, thereby substantiating the efficacy of the large patch training strategy.

V. CONCLUSION

In this paper, we propose large receptive-field transform coding with self-conditioned adaptability for learned image compression, which effectively captures more spatial correlations. To reduce channel-wise redundancy, we propose the self-conditioned channel transform to adjust the weight of each channel. To evaluate our proposed transform method, we align the entropy model with existing advanced non-linear transform coding techniques and obtain the models LLIC-STF, LLIC-ELIC, and LLIC-TCM. Extensive experiments demonstrate the superiority of our proposed large receptive field learning with self-conditioned adaptability. Our LLIC-STF, LLIC-ELIC, and LLIC-TCM achieve state-of-the-art performance and they reduce the BD-Rate by 9.49%, 9.47%, 10.94% on Kodak over VTM-17.0 Intra, respectively. To further enhance the performance, it is promising to integrate with more advanced entropy models [13], [14]. However, there are several limitations to be addressed. First, the complexities of the proposed LLIC models are not low enough, which means that they cannot be directly employed on mobile devices. Second, the learned image compression models are trained on natural images, which means that the generalization ability on out-of-distribution images (e.g., screen content) may be limited. The decoding complexity of LLIC models can be further reduced by employing asymmetric encoder-decoder structure [73], where the encoder could be heavy while the decoder is light. To enhance the generalization ability of learned image compression models, we suggest fine-tuning the encoder or latent representation for a specific input, which will increase the encoding time, but the decoding

complexity will still be low. In addition, fine-tuning the encoder or latent representation will also improve the performance on natural images. We will investigate these techniques in the future.

REFERENCES

- [1] J. Ballé, V. Laparra, and E. P. Simoncelli, "End-to-end optimized image compression," in *International Conference on Learning Representations*, 2017.
- [2] L. Theis, W. Shi, A. Cunningham, and F. Huszár, "Lossy image compression with compressive autoencoders," in *International Conference on Learning Representations*, 2017.
- [3] J. Ballé, D. Minnen, S. Singh, S. J. Hwang, and N. Johnston, "Variational image compression with a scale hyperprior," in *International Conference on Learning Representations*, 2018.
- [4] D. Minnen, J. Ballé, and G. D. Toderici, "Joint autoregressive and hierarchical priors for learned image compression," in *Advances in Neural Information Processing Systems*, 2018, pp. 10 771–10 780.
- [5] D. Minnen and S. Singh, "Channel-wise autoregressive entropy models for learned image compression," in *2020 IEEE International Conference on Image Processing (ICIP)*. IEEE, 2020, pp. 3339–3343.
- [6] S. Ma, X. Zhang, C. Jia, Z. Zhao, S. Wang, and S. Wang, "Image and video compression with neural networks: A review," *IEEE Transactions on Circuits and Systems for Video Technology*, vol. 30, no. 6, pp. 1683–1698, 2019.
- [7] Y. Zhu, Y. Yang, and T. Cohen, "Transformer-based transform coding," in *International Conference on Learning Representations*, 2022.
- [8] R. Zou, C. Song, and Z. Zhang, "The devil is in the details: Window-based attention for image compression," in *In Proceedings of the IEEE conference on computer vision and pattern recognition*, 2022.
- [9] X. Zhu, J. Song, L. Gao, F. Zheng, and H. T. Shen, "Unified multivariate gaussian mixture for efficient neural image compression," in *Proceedings of the IEEE/CVF Conference on Computer Vision and Pattern Recognition*, 2022, pp. 17 612–17 621.
- [10] A. B. Koyuncu, H. Gao, A. Boev, G. Gaikov, E. Alshina, and E. Steinbach, "Contextformer: A transformer with spatio-channel attention for context modeling in learned image compression," in *European Conference on Computer Vision*, 2022, pp. 447–463.
- [11] R. Feng, Z. Guo, W. Li, and Z. Chen, "Nvtc: Nonlinear vector transform coding," in *Proceedings of the IEEE/CVF Conference on Computer Vision and Pattern Recognition*, June 2023, pp. 6101–6110.
- [12] D. He, Z. Yang, W. Peng, R. Ma, H. Qin, and Y. Wang, "Elic: Efficient learned image compression with unevenly grouped space-channel contextual adaptive coding," in *Proceedings of the IEEE/CVF Conference on Computer Vision and Pattern Recognition*, June 2022, pp. 5718–5727.
- [13] W. Jiang, J. Yang, Y. Zhai, P. Ning, F. Gao, and R. Wang, "Mlic: Multi-reference entropy model for learned image compression," in *Proceedings of the 31st ACM International Conference on Multimedia*, 2023, pp. 7618–7627.
- [14] W. Jiang and R. Wang, "Mlic++: Linear complexity multi-reference entropy modeling for learned image compression," in *ICML 2023 Workshop Neural Compression: From Information Theory to Applications*, 2023. [Online]. Available: <https://openreview.net/forum?id=hx1pcSoz2t>
- [15] J. Liu, H. Sun, and J. Katto, "Learned image compression with mixed transformer-cnn architectures," in *Proceedings of the IEEE/CVF Conference on Computer Vision and Pattern Recognition*, 2023, pp. 14 388–14 397.
- [16] B. Bross, Y.-K. Wang, Y. Ye, S. Liu, J. Chen, G. J. Sullivan, and J.-R. Ohm, "Overview of the versatile video coding (vvc) standard and its applications," *IEEE Transactions on Circuits and Systems for Video Technology*, vol. 31, no. 10, pp. 3736–3764, 2021.
- [17] D. P. Kingma and M. Welling, "Auto-encoding variational bayes," in *International Conference on Learning Representations*, 2014.
- [18] J. Ballé, P. A. Chou, D. Minnen, S. Singh, N. Johnston, E. Agustsson, S. J. Hwang, and G. Toderici, "Nonlinear transform coding," *IEEE Journal of Selected Topics in Signal Processing*, vol. 15, no. 2, pp. 339–353, 2020.
- [19] G. Toderici, W. Shi, R. Timofte, L. Theis, J. Ballé, E. Agustsson, N. Johnston, and F. Mentzer, "Workshop and challenge on learned image compression (clic2020)," *CVPR*, 2020. [Online]. Available: https://data.vision.ee.ethz.ch/cvl/clic/professional_valid_2020.zip
- [20] Z. Cheng, H. Sun, M. Takeuchi, and J. Katto, "Learned image compression with discretized gaussian mixture likelihoods and attention modules," in *Proceedings of the IEEE/CVF Conference on Computer Vision and Pattern Recognition*, June 2020.

- [21] F. Chen, Y. Xu, and L. Wang, "Two-stage octave residual network for end-to-end image compression," in *Proceedings of the AAAI Conference on Artificial Intelligence*, vol. 36, 2022, pp. 3922–3929.
- [22] Y. Xie, K. L. Cheng, and Q. Chen, "Enhanced invertible encoding for learned image compression," in *Proceedings of the ACM International Conference on Multimedia*, 2021, pp. 162–170.
- [23] D. Wang, W. Yang, Y. Hu, and J. Liu, "Neural data-dependent transform for learned image compression," in *Proceedings of the IEEE/CVF Conference on Computer Vision and Pattern Recognition*, 2022, pp. 17 379–17 388.
- [24] W. Luo, Y. Li, R. Urtasun, and R. Zemel, "Understanding the effective receptive field in deep convolutional neural networks," *Advances in neural information processing systems*, vol. 29, 2016.
- [25] Y. Zhang, K. Li, K. Li, B. Zhong, and Y. Fu, "Residual non-local attention networks for image restoration," in *International Conference on Learning Representations*, 2018.
- [26] T. Chen, H. Liu, Z. Ma, Q. Shen, X. Cao, and Y. Wang, "End-to-end learnt image compression via non-local attention optimization and improved context modeling," *IEEE Transactions on Image Processing*, vol. 30, pp. 3179–3191, 2021.
- [27] J. Hu, L. Shen, and G. Sun, "Squeeze-and-excitation networks," in *Proceedings of the IEEE conference on computer vision and pattern recognition*, 2018, pp. 7132–7141.
- [28] G. Toderici, S. M. O'Malley, S. J. Hwang, D. Vincent, D. Minnen, S. Baluja, M. Covell, and R. Sukthankar, "Variable rate image compression with recurrent neural networks," in *International Conference on Learning Representations*, 2016.
- [29] G. Toderici, D. Vincent, N. Johnston, S. Jin Hwang, D. Minnen, J. Shor, and M. Covell, "Full resolution image compression with recurrent neural networks," in *Proceedings of the IEEE conference on Computer Vision and Pattern Recognition*, 2017, pp. 5306–5314.
- [30] A. Van den Oord, N. Kalchbrenner, L. Espeholt, O. Vinyals, A. Graves *et al.*, "Conditional image generation with pixelcnn decoders," *Advances in neural information processing systems*, vol. 29, 2016.
- [31] D. He, Y. Zheng, B. Sun, Y. Wang, and H. Qin, "Checkerboard context model for efficient learned image compression," in *Proceedings of the IEEE/CVF Conference on Computer Vision and Pattern Recognition*, 2021, pp. 14 771–14 780.
- [32] Z. Guo, Z. Zhang, R. Feng, and Z. Chen, "Causal contextual prediction for learned image compression," *IEEE Transactions on Circuits and Systems for Video Technology*, 2021.
- [33] J. Ballé, V. Laparra, and E. P. Simoncelli, "Density modeling of images using a generalized normalization transformation," *arXiv preprint arXiv:1511.06281*, 2015.
- [34] K. He, X. Zhang, S. Ren, and J. Sun, "Deep residual learning for image recognition," in *Proceedings of the IEEE conference on computer vision and pattern recognition*, 2016, pp. 770–778.
- [35] C. Shin, H. Lee, H. Son, S. Lee, D. Lee, and S. Lee, "Expanded adaptive scaling normalization for end to end image compression," in *European Conference on Computer Vision*, 2022, pp. 390–405.
- [36] M. Akbari, J. Liang, J. Han, and C. Tu, "Learned multi-resolution variable-rate image compression with octave-based residual blocks," *IEEE Transactions on Multimedia*, vol. 23, pp. 3013–3021, 2021.
- [37] G. Gao, P. You, R. Pan, S. Han, Y. Zhang, Y. Dai, and H. Lee, "Neural image compression via attentional multi-scale back projection and frequency decomposition," in *Proceedings of the IEEE/CVF International Conference on Computer Vision*, 2021, pp. 14 677–14 686.
- [38] Y. Chen, H. Fan, B. Xu, Z. Yan, Y. Kalantidis, M. Rohrbach, S. Yan, and J. Feng, "Drop an octave: Reducing spatial redundancy in convolutional neural networks with octave convolution," in *Proceedings of the IEEE/CVF international conference on computer vision*, 2019, pp. 3435–3444.
- [39] H. Ma, D. Liu, R. Xiong, and F. Wu, "iwave: Cnn-based wavelet-like transform for image compression," *IEEE Transactions on Multimedia*, vol. 22, no. 7, pp. 1667–1679, 2019.
- [40] A. Vaswani, N. Shazeer, N. Parmar, J. Uszkoreit, L. Jones, A. N. Gomez, Ł. Kaiser, and I. Polosukhin, "Attention is all you need," *Advances in neural information processing systems*, vol. 30, pp. 5998–6008, 2017.
- [41] Z. Liu, Y. Lin, Y. Cao, H. Hu, Y. Wei, Z. Zhang, S. Lin, and B. Guo, "Swin transformer: Hierarchical vision transformer using shifted windows," in *Proceedings of the IEEE/CVF International Conference on Computer Vision (ICCV)*, October 2021, pp. 10 012–10 022.
- [42] Y. Bai, X. Yang, X. Liu, J. Jiang, Y. Wang, X. Ji, and W. Gao, "Towards end-to-end image compression and analysis with transformers," in *Proceedings of the AAAI conference on artificial intelligence*, vol. 36, no. 1, 2022, pp. 104–112.
- [43] A. A. Jeny, M. S. Junayed, and M. B. Islam, "An efficient end-to-end image compression transformer," in *2022 IEEE International Conference on Image Processing (ICIP)*. IEEE, 2022, pp. 1786–1790.
- [44] M. Lu, P. Guo, H. Shi, C. Cao, and Z. Ma, "Transformer-based image compression," in *Data Compression Conference*, 2022, pp. 469–469.
- [45] M. Wang, K. Zhang, L. Zhang, Y. Li, J. Li, Y. Wang, and S. Wang, "End-to-end image compression with swin-transformer," in *2022 IEEE International Conference on Visual Communications and Image Processing (VCIP)*. IEEE, 2022, pp. 1–5.
- [46] W. B. Pennebaker and J. L. Mitchell, *JPEG: Still image data compression standard*. Springer Science & Business Media, 1992.
- [47] M. Rabbani, "Jpeg2000: Image compression fundamentals, standards and practice," *Journal of Electronic Imaging*, vol. 11, no. 2, p. 286, 2002.
- [48] G. J. Sullivan, J.-R. Ohm, W.-J. Han, and T. Wiegand, "Overview of the high efficiency video coding (hevc) standard," *IEEE Transactions on circuits and systems for video technology*, vol. 22, no. 12, pp. 1649–1668, 2012.
- [49] J. L. Ba, J. R. Kiros, and G. E. Hinton, "Layer normalization," *arXiv preprint arXiv:1607.06450*, 2016.
- [50] D. Hendrycks and K. Gimpel, "Gaussian error linear units (gelus)," *arXiv preprint arXiv:1606.08415*, 2016.
- [51] V. Nair and G. E. Hinton, "Rectified linear units improve restricted boltzmann machines," in *Proceedings of the 27th international conference on machine learning*, 2010, pp. 807–814.
- [52] L. Chen, X. Chu, X. Zhang, and J. Sun, "Simple baselines for image restoration," in *European Conference on Computer Vision*. Springer, 2022, pp. 17–33.
- [53] T.-Y. Lin, M. Maire, S. Belongie, J. Hays, P. Perona, D. Ramanan, P. Dollár, and C. L. Zitnick, "Microsoft coco: Common objects in context," in *European Conference on Computer Vision*, 2014, pp. 740–755.
- [54] J. Deng, W. Dong, R. Socher, L.-J. Li, K. Li, and L. Fei-Fei, "Imagenet: A large-scale hierarchical image database," in *2009 IEEE conference on computer vision and pattern recognition*. Ieee, 2009, pp. 248–255.
- [55] E. Agustsson and R. Timofte, "Ntire 2017 challenge on single image super-resolution: Dataset and study," *2017 IEEE Conference on Computer Vision and Pattern Recognition Workshops*, pp. 1122–1131, 2017.
- [56] B. Lim, S. Son, H. Kim, S. Nah, and K. Mu Lee, "Enhanced deep residual networks for single image super-resolution," in *Proceedings of the IEEE conference on computer vision and pattern recognition workshops*, 2017, pp. 136–144.
- [57] A. Paszke, S. Gross, F. Massa, A. Lerer, J. Bradbury, G. Chanan, T. Killeen, Z. Lin, N. Gimelshein, L. Antiga *et al.*, "Pytorch: An imperative style, high-performance deep learning library," in *Advances in Neural Information Processing Systems*, 2019, pp. 8024–8035.
- [58] J. Bégin, F. Racapé, S. Feltman, and A. Pushparaja, "Compressai: a pytorch library and evaluation platform for end-to-end compression research," *arXiv preprint arXiv:2011.03029*, 2020.
- [59] E. Kodak, "Kodak lossless true color image suite (photocd pcd0992)," 1993. [Online]. Available: <http://r0k.us/graphics/kodak/>
- [60] Z. Cheng, H. Sun, M. Takeuchi, and J. Katto, "Energy compaction-based image compression using convolutional autoencoder," *IEEE Transactions on Multimedia*, vol. 22, no. 4, pp. 860–873, 2020.
- [61] W. Yin, Y. Shi, W. Zuo, and X. Fan, "A co-prediction-based compression scheme for correlated images," *IEEE Transactions on Multimedia*, vol. 22, no. 8, pp. 1917–1928, 2020.
- [62] Y. Mei, L. Li, Z. Li, and F. Li, "Learning-based scalable image compression with latent-feature reuse and prediction," *IEEE Transactions on Multimedia*, vol. 24, pp. 4143–4157, 2022.
- [63] Y. Qian, Z. Tan, X. Sun, M. Lin, D. Li, Z. Sun, L. Hao, and R. Jin, "Learning accurate entropy model with global reference for image compression," in *International Conference on Learning Representations*, 2020.
- [64] N. Asuni and A. Giachetti, "Testimages: a large-scale archive for testing visual devices and basic image processing algorithms," in *STAG: Smart Tools & Apps for Graphics (2014)*, 2014.
- [65] G. Pan, G. Lu, Z. Hu, and D. Xu, "Content adaptive latents and decoder for neural image compression," in *European Conference on Computer Vision*, 2022, pp. 556–573.
- [66] G. Toderici, W. Shi, R. Timofte, L. Theis, J. Ballé, E. Agustsson, N. Johnston, and F. Mentzer, "Workshop and challenge on learned image compression (clic2021)," *CVPR*, 2021. [Online]. Available: https://storage.googleapis.com/clic2021_public/professional_test_2021.zip
- [67] JPEG-AI, "Jpeg-ai test images," https://jpegai.github.io/test_images/, 2020.
- [68] G. Bjontegaard, "Calculation of average psnr differences between rd-curves," *VCEG-M33*, 2001.

- [69] J. Liu, D. Liu, W. Yang, S. Xia, X. Zhang, and Y. Dai, “A comprehensive benchmark for single image compression artifact reduction,” *IEEE Transactions on image processing*, vol. 29, pp. 7845–7860, 2020.
- [70] Y. Qian, M. Lin, X. Sun, Z. Tan, and R. Jin, “Entroformer: A transformer-based entropy model for learned image compression,” in *International Conference on Learning Representations*, 2022.
- [71] Z. Wang, E. P. Simoncelli, and A. C. Bovik, “Multiscale structural similarity for image quality assessment,” in *The Thrity-Seventh Asilomar Conference on Signals, Systems & Computers*, 2003, vol. 2. Ieee, 2003, pp. 1398–1402.
- [72] X. Ding, X. Zhang, J. Han, and G. Ding, “Scaling up your kernels to 31x31: Revisiting large kernel design in cnns,” in *Proceedings of the IEEE/CVF conference on computer vision and pattern recognition*, 2022, pp. 11 963–11 975.
- [73] Y. Yang and S. Mandt, “Computationally-efficient neural image compression with shallow decoders,” in *Proceedings of the IEEE/CVF International Conference on Computer Vision (ICCV)*, 2023, pp. 530–540.